International Journal of Heat and Mass Transfer 51 (2008) 6268–6282

Contents lists available at ScienceDirect

International Journal of Heat and Mass Transfer

journal homepage: www.elsevier.com/locate/ijhmt

Bubble departure frequency in forced convective subcooled boiling flow

R. Situ [a,*,1], M. Ishii [b], T. Hibiki [b], J.Y. Tu [a], G.H. Yeoh [c], M. Mori [d]

[a] RMIT University, School of Aerospace, Mechanical and Manufacturing Engineering, PO Box 71, Bundoora, Victoria 3083, Australia
[b] School of Nuclear Engineering, Purdue University, 400 Central Drive, West Lafayette, IN 47907-2017, USA
[c] Nuclear Technology Division, Australian Nuclear Science Technology Organization, PMB 1, Menai, NSW 2234, Australia
[d] R&D Center, Tokyo Electric Power Company, 4-1 Egasaki, Tsurumi, Yokohama, Kanagawa 230-8510, Japan

ARTICLE INFO

Article history:
Received 11 December 2006
Received in revised form 18 April 2008
Available online 12 June 2008

Keywords:
Subcooled boiling
Bubble departure frequency
Flow visualization
Forced convection
Bubble waiting time
Bubble growth time
Bubble departure size

ABSTRACT

Forced convective subcooled boiling flow experiments were conducted in a vertical upward annular channel. Water was used as the testing fluid, and the tests were performed at atmospheric pressure. A high-speed digital video camera was applied to capture the dynamics of the bubble nucleation process. Bubble departure frequencies were obtained from the video for a total of 58 test conditions. The non-dimensional analysis was performed on the current data as well as available data from literature. Existing models and correlations were compared with the experimental data of bubble waiting time, growth time, and departure frequency. The correlations developed for pool boiling flow do not work well for forced convective subcooled boiling flow, while the models proposed for subcooled boiling flow cannot predict the bubble departure frequency in wide experimental ranges. Dimensionless bubble departure frequency is correlated with non-dimensional nucleate boiling heat flux. The new correlation agrees reasonably well with existing experimental data at lower wall superheat.

1. Introduction

The subcooled boiling region is characterized, in convective flow boiling, as boiling occurring close to the heated wall while the remaining bulk of the fluid is subcooled. Bubbles will be rapidly condensed if they move out of the developing saturation layer. In the subcooled region, there exists a small void fraction. Gradually, as the bulk is heated by conduction and convection, the saturation layer expands and eventually covers the entire flow channel. Subcooled boiling flow comprises all the interactive, complicated, and dynamic processes such as hydrodynamics, heat and mass transfer, nucleation, departure, coalescence and breakup of bubbles. Many industrial applications, for instance, boiler, boiling water reactor, and the new generation of electronic and computer system, are seriously interested in the understanding and modeling of subcooled boiling.

In spite of enormous efforts, bubble nucleation and departure in subcooled boiling flow still pose a challenge work. Bubble nucleation happens within the small activated cavities at the heater surface when the wall temperature exceeds the saturation temperature of the liquid at the local pressure. Bubbles subsequently detach from the nucleation site due to the forces acting on them in the axial and normal directions. Two important parameters associated with departure are the bubble departure frequency and bubble departure size, which are defined as the frequency and size of bubble when departing from the nucleation cavities, respectively.

The bubble departure phenomena in pool boiling have been studied since 1950s. Zuber [1] found that bubble departure and the flow regimes are similar to the formation of gas bubbles at orifices. According to Zuber [2], three regimes of vapor bubble departure from the nucleation site can be discerned: (1) Laminar regime: When vapor flow rates are very low, bubbles rise at a constant velocity, and do not interact with each other. The bubble diameter is almost independent of vapor flow rate, and the bubble departure frequency increases with increasing vapor flow rate. This regime is also referred as the region of static, separated or isolated bubbles. (2) Turbulent regime: When vapor flow rates are intermediate, the bubble departure diameter increases with flow rate while bubble departure frequency remains constant. A bubble interacts and may coalesce with its predecessor above the nucleation site, and the bubble size is non-uniform. This regime is also referred as the region of multiple or interfering bubbles. (3) When vapor flow rates are even higher, a swirling vapor stream is generated at the nucleation site. The vapor jet is similar to a tornado or a waterspout. The current study focuses on the bubble departure phenom-

* Corresponding author. Tel.: +61 7 31382452; fax: +61 7 31388381.
E-mail address: situ@qut.edu.au (R. Situ).
[1] Current address: School of Engineering Systems, Queensland University of Technology, GPO Box 2434, Brisbane, Queensland 4001, Australia.

0017-9310/$ - see front matter © 2008 Elsevier Ltd. All rights reserved.
doi:10.1016/j.ijheatmasstransfer.2008.04.028

Nomenclature

A	area
b	constant
C_{ev}	coefficient
C_p	specific heat at constant pressure
D	diameter
F_d	drag force
F_{du}	unsteady drag force (growth force)
F_g	gravity force
F_p	pressure force
F_{qs}	quasi-steady force
F_s	surface tension force
F_{sl}	shear lift force
f_d	bubble departure frequency
G	mass flux
g	gravitational acceleration
h	heat transfer coefficient
i_{fg}	heat of vaporization (latent heat)
Ja	Jacob number
k	thermal conductivity
N_a	active nucleation site density
N_{fd}	dimensionless bubble departure frequency
N_{fG}	inverse of dimensionless bubble growth time
N_{fW}	inverse of dimensionless bubble waiting time
N_q	dimensionless heat flux
N_{qFC}	dimensionless single-phase forced convective heat flux
N_{qG}	dimensionless heat flux using bubble departure diameter
N_{qNB}	dimensionless nucleate boiling heat flux
N_{qW}	dimensionless heat flux using cavity diameter
p	pressure
Pr_f	liquid Prandtl number
q''	heat flux
r	radius
Re	Reynolds number
S	suppression factor
T	temperature
T_0	bubble surface temperature
t	time
u	velocity

Greek symbols

α	thermal diffusivity
δ	thermal layer thickness
θ_i	inclination angle
ρ	density
σ	surface tension
μ	viscosity

Subscripts

b	bubble or bulk
c	cavity or convective
d	departure
e	effective
ev	evaporation
f	liquid phase
FC	forced convective
G	growth
g	vapor phase
H	hydraulic
h	heated
NB	nucleate boiling
r	relative
s	saturation
sub	subcooling
W	waiting
w	wall
x	coordinate
y	coordinate

ena in subcooled boiling condition, which falls in the laminar and turbulent regimes.

Literature review shows that bubble departure frequency at pool boiling have been studied extensively. Jokob [3] found that the product of bubble departure frequency and departure diameter to be a constant. Zuber [4] correlated this constant to be half of the bubble rising velocity in a gravitational field. Ivey [5] offered three correlations with the product of departure frequency and different power of departure diameter for three regions: (1) hydrodynamic region in which buoyancy and drag forces predominate; (2) transition region where buoyancy, drag, and surface tension forces are in the same order; and (3) thermodynamic region where bubble growth dominates. In literature, researchers also attempted to mechanistically model the bubble departure frequency in pool boiling. The first step is to divide the reciprocal of departure frequency, i.e., one nucleation cycle, into two parts. In one nucleation cycle, there exists a waiting time, i.e., t_W, defined as the period from the moment of the former bubble departs to the moment of the current bubble nucleates, and a growth time, t_G, which is defined as the period from the moment of bubble appearance until the moment of bubble departure. Han and Griffith [6] proposed that the waiting time from the criterion of bubble nucleation and potential flow theory. While for bubble growth time, Hatton and Hall [7] offered a model by taking account of the bubble departure diameter and thermally-controlled bubble growth rate.

Recently, several investigations have been performed on the bubble departure frequency in convective boiling. Thorncroft et al. [8] reported bubble waiting time and departure diameter of electronic fluid FC-87 under vertical up-flow and down-flow boiling in a 12.7 mm ID square duct with one side heated by a 30 cm-length nichrome strip. The data were captured at mass flux varying from 190 to 666 kg/m^2 s, heat flux changing from 1.32 to 14.6 kW/m^2, and bulk subcooling ranging from 1.0 to 5.0 °C. Basu et al. [9,10] measured waiting time, growth time, departure size and frequency in an upward-vertical subcooled flow boiling facility using water as working fluid. The experimental data were taken at pressure of 0.103 MPa, mass fluxes from 235 to 684 kg/m^2 s, and heat flux changing from 160 to 963 kW/m^2. The test section is almost square in cross section with 16.33 cm^2 in flow area. The heated surface is a 3.175 cm × 30.5 cm flat copper plate with contact angle varying from 30° to 90°. The waiting time was correlated against wall superheat, while the growth time was correlated with bulk subcooling, bubble departure diameter, and superheated liquid layer. It shall be noted that the correlation is proposed for limited test scope and heated surface. Podowski et al. [11] proposed mechanistic models for both waiting time and growth time. However, the model has not been directly validated.

In summary, few works have been attempted to examine the existing correlations and models of bubble departure frequency in forced convective subcooled boiling conditions, where both experimental and analytical works are deficient. Hence the purpose of this paper is to study the bubble departure frequency in vertical upward forced-convective subcooling boiling flow. The investigation will be carried out by performing experimental test, and analyzing the existing experimental data and model/correlation in literature.

2. Literature survey

2.1. Analytical work

Several models and correlations were found in literature to predict bubble departure frequency for pool boiling and flow boiling. In addition, bubble departure frequency can be deemed as the reciprocal of the summation of bubble waiting time and bubble growth time:

$$f_d = 1/(t_W + t_G). \tag{1}$$

The models of bubble waiting time and growth time are discussed as following sections.

2.1.1. Pool boiling

2.1.1.1. Bubble waiting time. Based on the criterion of bubble nucleation and potential flow theory, Han and Griffith [6] proposed that the waiting time to be the heating time needed for the thermal layer thickness equivalent with 3/2 times of the cavity radius

$$t_W = \frac{\delta^2}{\pi\alpha_f} = \frac{9}{16\pi\alpha_f}\left\{\frac{2(T_w - T_b)r_c}{T_w - T_s[1 + (4\sigma/D_c\rho_g i_{fg})]}\right\}^2 \quad \text{or}$$
$$N_{fW} \equiv \frac{D_c^2}{\alpha_f t_W} = \frac{16\pi}{9}\left\{\frac{T_w - T_s[1 + (2\sigma/r_c\rho_g i_{fg})]}{(T_w - T_b)}\right\}^2, \tag{2}$$

where δ, α_f, T_w, T_b, r_c, T_s, σ, ρ_g, and i_{fg} are thermal layer thickness, thermal diffusivity of liquid, wall temperature, bulk liquid temperature, cavity radius, saturation temperature, surface tension, vapor density and latent heat, respectively. N_{fW} is the inverse of dimensionless bubble waiting time. The waiting time was not compared with data because the cavity radius was not available. However, by putting the fluid temperature line and bubble equilibrium temperature curve tangent to each other, Han and Griffith deduced the minimum waiting time to be

$$t_{W,min} = \frac{\delta_{min}^2}{\pi\alpha_f} = \frac{144(T_w - T_b)^2 T_s^2 \sigma^2}{\pi\alpha_f \rho_g^2 i_{fg}^2 (T_w - T_s)^4}. \tag{3}$$

Furthermore, the bubble waiting time was measured by Han and Griffith [6] from water pool boiling with heated gold surface at atmosphere pressure. The experiments show that the waiting time changes from 17 to 130 time of the minimum waiting time $t_{W,\,min}$.

2.1.1.2. Bubble growth time. From the definition of bubble growth time, it can be estimated when the bubble growth rate and departure diameter are known. Zuber [12] proposed a correlation of bubble growth in non-uniform temperature fields:

$$r_b = 2bJa\sqrt{\alpha_f t}/\sqrt{\pi}, \tag{4}$$

where b is a constant between 1 and $\sqrt{3}$, and Ja is Jacob number defined as

$$Ja \equiv \rho_f C_{pf}(T_0 - T_s)/(\rho_g i_{fg}), \tag{5}$$

where ρ_f, C_{pf}, T_0 are liquid density, specific heat of liquid, and bubble surface temperature. Zeng et al. [13] found that for horizontal flow boiling of R113, at liquid velocity $u_f = 0.30$ m/s, wall superheat $\Delta T_w = 8.2$ °C, and saturation temperature $T_s = 67$ °C, $b = 1.73$ has the best fit for bubble growth rate within ±7.68%. The bubble growth time is therefore obtained from

$$N_{fG} \equiv \frac{D_d^2}{\alpha_f t_G} = \frac{16b^2}{\pi} Ja_w^2 = \frac{16b^2}{\pi}\left[\frac{\rho_f C_{pf}(T_w - T_s)}{\rho_g i_{fg}}\right]^2. \tag{6}$$

N_{fG} is the inverse of dimensionless bubble growth time. Hatton and Hall [7] used Plesset and Zwick's growth rate [14] to deduce the bubble growth time as

$$t_G = \frac{\pi\alpha_f}{3}\left[\frac{(i_{fg}\rho_g)^2 D_d r_c}{8k_f\sigma T_s}\right]^2 \quad \text{or} \quad N_{fG} \equiv \frac{D_d^2}{\alpha_f t_G} = \frac{3}{\pi}\left[\frac{8k_f\sigma T_s}{(i_{fg}\rho_g)^2\alpha_f r_c}\right]^2. \tag{7}$$

The model was compared with water pool boiling data at 0.0662 and 0.101 MPa as pressure where waiting time is found to be negligible, and the averaged prediction error is ±60.2%.

2.1.1.3. Bubble departure frequency. Cole [15] assumed that in hydrodynamic region, where buoyancy and drag forces dominate, the product of bubble departure diameter and frequency is equal to bubble rise velocity, which is derived from force balance of buoyancy force and drag force. The departure frequency can be given by

$$N_{fd1} \equiv f_d D_d^{1/2}/g^{1/2} = \sqrt{4(\rho_f - \rho_g)/(3\rho_f)}, \tag{8}$$

where g is gravitational acceleration. The model agrees reasonably well but tends to over-predict with water, CCl_4, and methanol data with averaged error of ±52.2%.

Similarly, Zuber [4] assumed that the quotient of departure diameter divided by growth time equals the bubble rise velocity in a gravitational field, and bubble growth time is almost equal to waiting time. The following equation was obtained as

$$N_{fd2} \equiv \frac{f_d D_d}{u_b} = \frac{f_d D_d}{1.18[\sigma g(\rho_f - \rho_g)/\rho_f^2]^{1/4}} = 0.5, \tag{9}$$

where u_b is bubble rise velocity. The correlation agreed satisfactorily with data of water, CCl_4, and methanol on horizontal pool boiling with ±20.4% as averaged uncertainty.

Hatton and Hall [7] assumed that waiting time is negligible compared with growth time. Hence, by adopting the same form as in Eq. (7), the departure frequency and the square power of bubble departure diameter were correlated from pool boiling data of water, at pressure of 0.0162, 0.0662, and 0.101 MPas, with prediction error of ±34.3%:

$$N_{fd3} \equiv f_d D_d^2/\alpha_f = 284.7. \tag{10}$$

As described in introduction, Ivey [5] proposed three correlations for different regions:

(1) Hydrodynamic region (correlated with water and methanol data at ±14.0% error)

$$N_{fd1} = f_d \cdot D_d^{1/2}/g^{1/2} = 0.90. \tag{11}$$

(2) Transition region (correlated with water, methanol, isopropanol, and carbon tetrachloride data at averaged error of ±14.3%)

$$f_d \cdot D_d^{3/4}/g^{1/4} = 0.44\ \text{cm}^{1/4}. \tag{12}$$

(3) Thermodynamic region (correlated with water data at averaged error of ±6.87%)

$$f_d \cdot D_d^2 = \text{constant}\ \text{m}^2/\text{s}. \tag{13}$$

2.1.2. Forced convective flow boiling

2.1.2.1. Basu's correlation. Basu et al. [10] proposed the correlation of bubble waiting time and growth time from their flow boiling data with mass flux from 235.0 to 684.0 kg/m^2 s, inlet subcooling from 7.7 to 46.5 °C, and heat flux from 200.0 to 454.0 kW/m^2. The waiting time was correlated with wall superheat with the averaged prediction accuracy of ±23.2%.

$$t_W = 139.1(\Delta T_w^{-4.1}). \tag{14}$$

In addition, the bubble growth time was correlated with departure diameter, wall superheat and bulk subcooling with the averaged uncertainty of prediction ±9.99%:

$$N_{fG} \equiv D_d^2/(\alpha_f t_G) = 45 Ja_w \exp(-0.02 Ja_{sub}), \quad (15)$$

$$Ja_w \equiv \rho_f C_{pf}(T_w - T_s)/(\rho_g i_{fg}), \quad \text{and} \quad Ja_{sub} \equiv \rho_f C_{pf}(T_s - T_b)/\rho_g i_{fg}. \quad (16)$$

2.1.2.2. Podowski et al.'s model. Podowski et al. [11] proposed a mechanistic model of bubble departure frequency for forced convection subcooled boiling. A rigorous analytical solution of bubble waiting time was obtained by balancing transient heat transfer in the heated wall and from the wall to the liquid. The model described the wall temperature at nucleation site as an instantaneous fluctuating parameter, which is reasonably nevertheless not predicted by other models or empirical correlation in the literature. The bubble waiting time is therefore given by

$$t_W = \left[\left(-C_2 + \sqrt{C_2^2 - 4C_1C_3}\right)/2C_1\right]^2, \quad (17)$$

where

$$C_2 = \left(\frac{k_w T_w}{\sqrt{\alpha_w}} + \frac{k_f T_b}{\sqrt{\alpha_f}}\right) \Big/ \left(\frac{k_w}{\sqrt{\alpha_w}} + \frac{k_f}{\sqrt{\alpha_f}}\right) - T_s - \frac{q''_w r_c}{R\sqrt{\pi\alpha_f}} - \frac{2\sigma}{r_c}\frac{T_s(1/\rho_g - 1/\rho_f)}{i_{fg}},$$

$$C_1 = \frac{2q''_w}{R\pi},$$

$$C_3 = -\lfloor (k_w T_w/\sqrt{\alpha_w} + k_f T_b/\sqrt{\alpha_f})/(k_w/\sqrt{\alpha_w} + k_f/\sqrt{\alpha_f}) - T_b \rfloor r_c/\sqrt{\pi\alpha_f},$$

$R = k_w/\sqrt{\pi\alpha_w} + k_f/\sqrt{\pi\alpha_f}$, k_w is thermal conductivity, and α_w is thermal diffusivity of wall. In addition, theoretical investigation has also been performed by Podowski et al. [11] to deduce the bubble growth time

$$t_G = \left[\left(-A_2 + \sqrt{A_2^2 - 4A_1A_3}\right)/2A_1\right]^2, \quad (18)$$

where

$$A_2 = 2\lfloor (k_w T_w/\sqrt{\alpha_w} + k_f T_b/\sqrt{\alpha_f})/(k_w/\sqrt{\alpha_w} + k_f/\sqrt{\alpha_f}) + 2q''_w\sqrt{t_W}/R\pi - T_s \rfloor/\sqrt{\pi\alpha_w}, \quad A_1 = q''_w/k_w, \quad \text{and}$$

$$A_3 = D_d \rho_g i_{fg}/2k_w.$$

The above discussed models and correlations are summarized in Table 1. The major assumptions and dimensionless parameters are exhibited as well. These parameters will be discussed to derive the dominant parameters determining the bubble departure frequency.

2.1.3. Dominant parameters and their physical meanings

To have a better understanding of the relationship between bubble departure frequency and other parameters, the dominant dimensionless number shall be formed. Ivey [5] suggested that in thermal-dynamic region, bubble diameter is in the same order of magnitude as the thermal boundary-layer thickness δ, which can be given as

$$\delta = 1.6(\pi\alpha_f t_b)^{1/2}, \quad (19)$$

where t_b is the period of single bubble. Noting that $t_b = 1/f_d$, it might deduce the dimensionless bubble departure frequency as

$$N_{fd} = N_{fd3} \equiv f_d D_d^2/\alpha_f = \text{constant}. \quad (20)$$

The other two dimensionless numbers of bubble departure frequency might be deduced from Eqs. (8), (9) and (11):

$$N_{fd1} \equiv f_d D_d^{1/2}/g^{1/2}, \quad \text{and} \quad N_{fd2} \equiv f_d D_d/u_b \quad (21)$$

for pool boiling hydrodynamic region where buoyancy and drag forces are dominant forces. However, in forced convective flow boiling, the force balance on the bubble is far different from pool boiling. Hence the dimensionless numbers in Eq. (21) will not be used for further analysis. Furthermore, Eqs. (2) and (10) suggests that the inverse of dimensionless bubble waiting time and growth time can be defined as

$$N_{fW} \equiv D_c^2/(\alpha_f t_G), \quad \text{and} \quad N_{fG} \equiv D_d^2/(\alpha_f t_G). \quad (22)$$

So far the bubble departure frequency, waiting time and growth time, can be non-dimensionalized as shown in Eqs. (20) and (22), respectively. Next we need to discuss the dominant parameters determining these three dimensionless numbers. In forced convective flow boiling, the essential boundary conditions affecting bubble nucleation, growth, and departure are mass flux, wall superheat and heat flux. The first two parameters can be represented by the Jacob number, Ja_w, as shown in Eq. (16) and liquid Reynolds number

$$Re_f \equiv \rho_f u_f D_H/\mu_f, \quad (23)$$

where u_f, D_H, μ_f are liquid velocity, hydraulic diameter, and liquid viscosity, respectively. Another dimensionless group governing the heat flux can be deduced from Podowski et al's waiting time model and growth time model from Eqs. (17) and (18):

$$N_q \equiv q''_w\sqrt{\pi\alpha t}/(k\Delta T_w), \quad (24)$$

where q''_w is wall heat flux. Equations in Eq. (22) imply that the term $\sqrt{\pi\alpha t}$ can be replaced by length scales, such as cavity diameter D_c or bubble departure diameter D_d. In addition, wall superheat also appears in the denominator, which complicates this number. Hence, Eq. (24) is multiplied with Jacob number and the square root of equations in Eq. (22) to be

$$N_{qW} \equiv N_q \cdot Ja_w \cdot \sqrt{\frac{N_{fW}}{\pi}} = \frac{q''_w D_c}{\alpha_f \rho_g i_{fg}}, \quad \text{and}$$

$$N_{qG} \equiv N_q \cdot Ja_w \cdot \sqrt{\frac{N_{fG}}{\pi}} = \frac{q''_w D_d}{\alpha_f \rho_g i_{fg}}. \quad (25)$$

To sum up, N_{qW} as well as Re_f and Ja_w may affect the bubble waiting time, while N_{qG} with Re_f and Ja_w would have an influence on bubble growth time.

2.2. Experimental work

Basu and her colleague [9,10] measured waiting time, growth time, and departure size and frequency in an upward-vertical subcooled flow boiling facility with water as working fluid. The experimental data were taken at a pressure of 0.103 MPa, mass fluxes from 235 to 684 kg/m^2 s, and heat flux changing from 160 to 963 kW/m^2. The test section is almost square in cross section with 16.33 cm^2 in flow area. The heated surface is a 3.2 cm × 30.5 cm flat copper plate with contact angle varying from 30° to 90°. The measured parameters are mass flux, inlet liquid temperature, heat flux, contact angle, bubble departure frequency, bubble waiting time, bubble growth time, and bubble departure size, etc. The measurement uncertainties for heat flux, bubble diameter, liquid temperature, wall temperature, and contact angle are ±1.5 to ± 9.4%, ±12%, ±0.4 to ±0.8 %, ±0.2%, and ±3.0°, respectively.

Thorncroft et al. [8] collected bubble waiting time and bubble departure diameter of electronic fluid FC-87 under vertical up-flow and down-flow boiling in a 12.7 mm ID square duct with one side heated by a 30 cm-length ×12.7 mm-width ×0.15 mm-thickness nichrome strip. The data were captured at isolated boiling with mass flux varying from 190 to 666 kg/m^2 s, heat flux changing from 1.32 to 14.6 kW/m^2, and bulk subcooling ranging from 1.0 to 5.0 °C.

Table 1
Summary of models and correlations in literature

Flow conditions	Parameters	Investigators	Equation	Major assumptions	Dimensionless parameters
Pool boiling	Bubble waiting time	Han & Griffith [6]	Eq. (2)	Waiting time is the heating time for 3/2 times of the cavity diameter	$D_c^2/\alpha_f t_W$
	Bubble growth time	Zuber [12]	Eq. (6)	Bubble growth in non-uniform temperature field	$D_d^2/\alpha_f t_G$
		Hatton & Hall [7]	Eq. (7)	Thermally controlled bubble growth	$D_d^2/\alpha_f t_G$
	Bubble departure frequency	Cole [15]	Eq. (8)	Hydrodynamic region where buoyancy and drag force dominate	$f_d D_d^{1/2}/g^{1/2}$
		Zuber [4]	Eq. (9)	D_d/t_G = bubble rise velocity; $t_G = t_W$	$f_d D_d/u_b$
		Hatton & Hall [7]	Eq. (10)	$t_W = 0$	$f_d D_d^2/\alpha_f$
		Ivey [5]	Eq. (11)	Buoyancy and drag forces dominate	$f_d D_d^{1/2}/g^{1/2}$
		Ivey [5]	Eq. (12)	Buoyancy, drag, and surface tension forces are in same order	N/A
		Ivey [5]	Eq. (13)	Bubble growth dominates	N/A
Forced convective boiling	Bubble waiting time	Basu et al. [10]	Eq. (14)	Correlated with wall superheat	N/A
		Podowski et al. [11]	Eq. (17)	Transient 1-D heat conduction in heated wall and liquid	$q''_w\sqrt{\pi\alpha t_W}/k\Delta T_w$
	Bubble growth time	Basu et al. [10]	Eq. (15)	Correlation with departure diameter, wall superheat and bulk subcooling	$D_d^2/\alpha_f t_G$
		Podowski et al. [11]	Eq. (18)	Local surface temperature close to saturation temperature; heat flux from wall is solely used for evaporation.	$q''_w\sqrt{\pi\alpha t_G}/k\Delta T_w$

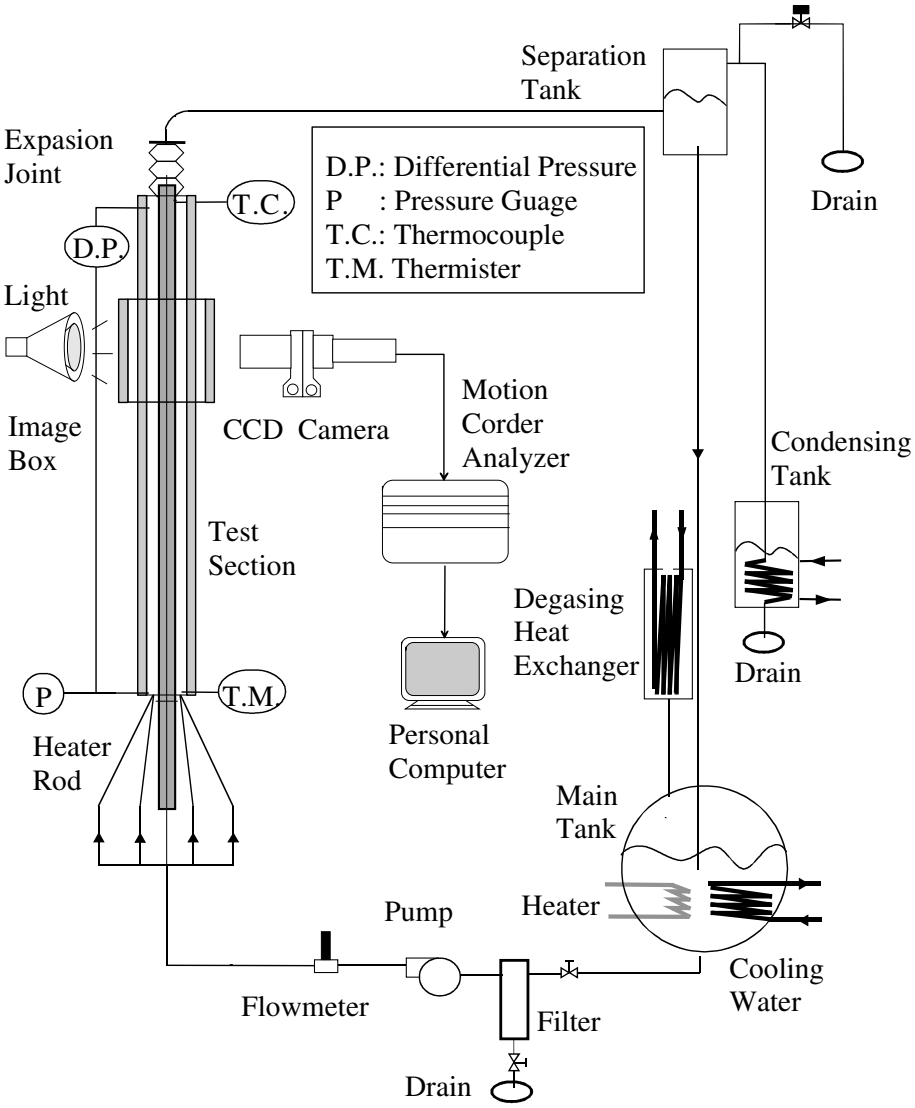

Fig. 1. Schematic diagram of experimental loop.

The other measured parameters are pressure, saturate temperature, wall superheat, bulk subcooling, heat flux, convective heat transfer coefficient, and lift-off diameter, etc. Interestingly, the plotted bubble mean growth curves can lead to the estimation of bubble growth time and hence bubble departure frequency. The measurement accuracies for mass flux, heat flux, pressure, temperature, and bubble diameter are ±0.5% of full scale, ±1%, ±0.5°C, and 20 μm, respectively.

3. Experiment

3.1. Experimental facility

An experimental facility has been designed to measure the relevant two-phase parameters necessary for developing constitutive models for the two-fluid model in subcooled boiling flow. The experimental facility is a scaled-down loop from a prototypic boiling water reactor based on proper scaling criteria for geometric, hydrodynamic, and thermal similarities [16,17]. The schematic diagram of the flow loop is shown in Fig. 1. The subcooled water is held in the main tank. The main tank has a cartridge heater and heat exchanger to control the test-section-inlet subcooling. The water is pumped by a positive displacement pump and divided into four separate lines. Each line runs to a fitting that is connected to the bottom of the test section. The test section is an annulus formed by a clear polycarbonate tube on the outside with an ID of 38.1 mm, and a cartridge heater on the inside with an OD of 19.1 mm. Thus, the hydraulic equivalent diameter, D_H, is 19.1 mm. The heater has an overall length of 2670 mm with a heated section of 1730 mm in length. The distance between the test section inlet and the heating section inlet is 212 mm. The maximum power of the heater is 20 kW that corresponds to a maximum heat flux of 0.193 MW/m^2. At the top of the test section, an expansion joint is installed to accommodate the thermal expansion of the polycarbonate test section. A separation tank is used to separate vapor phase from water. The steam is then condensed, and the water is returned to the main tank. The separation tank is located directly above the main tank. The detailed description of the experimental facility and experimental setup are found in our previous papers [18,19].

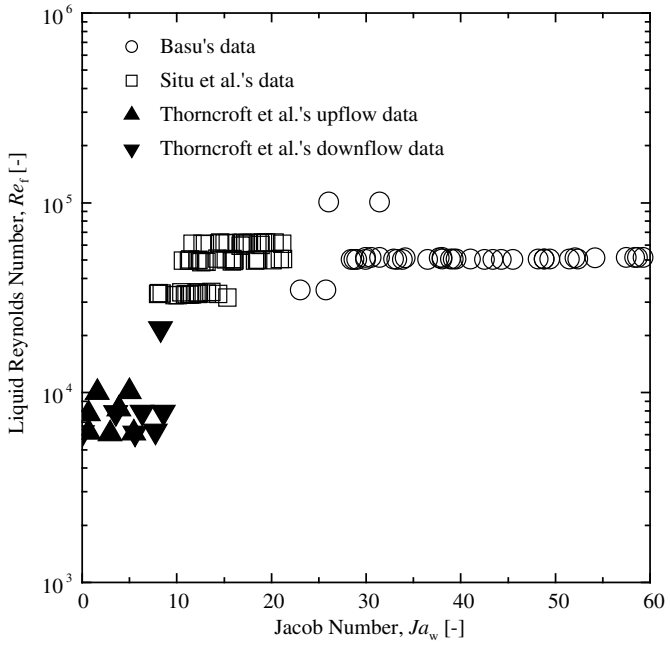

Fig. 2. Comparison of wall temperature correlation with Basu's data.

3.2. Experimental conditions

Experiments of 58 conditions are performed for the study of the bubble departure frequency though flow visualization [20]. The inlet temperature ranges from 80.0 to 98.5 °C; the inlet velocity varies from 0.487 to 0.939 m/s; and the heat flux changes from 60.7 to 206 kW/m^2. Compared with the test conditions by Basu [9,10], the current tests are conducted with higher mass flux and lower heat flux. The other major differences are flowing channel geometry (annulus vs. almost square), heated surface (stainless steel rod vs. copper flat plat).

At every steady-state experimental condition, the heater power, inlet water temperature, and inlet water velocity are chosen in such a way that a stable active nucleation site is observed and can be captured by the high-speed video camera. The experiments are performed at atmosphere pressure. The local wall temperature is not measured because the heated surface is a commercially-made heater rod. Furthermore, experimental observation finds that the bubble departure is a quick and continuous process. Bubble starts to slide along the heated surface once it appears, and it is rather difficult to determine the moment of bubble departure. Hence, the exact bubble departure size is not measured in the present study, but it is estimated by analyzing the images to be between 0.1 and 0.4 mm.

The inlet temperature is measured by the thermistor probe with interchangeable sensor accuracy of ±0.1 °C. The pressure drop cross the test section was measured by Honeywell ST 3000 Smart Transmitter. The combined zero and span inaccuracy for the differential pressure cell is ±0.4% of span. Heat flux and inlet velocity are acquired by a data acquisition system. The measurement accuracies of heat flux, liquid temperature, liquid velocity, pressure, and differential pressure are ±1%, ±0.1 °C, ±1%, ±1% full-scale reading (55 kPa), and ±1% full-scale reading (6.9 kPa), respectively.

4. Results and discussion

To examine the bubble departure frequency in a broad experimental range, the analysis includes Basu's experimental data [9], the data taken in the current annulus test section (referred as Situ et al.'s data in all the figures) and Thorncroft et al.'s data [8]. Fig. 2 plots all the experimental conditions in the map of Re_f vs. Ja_w, because liquid velocity and wall superheat might be the crucial boundary parameters controlling the bubble departure frequency. In this figure and the rest of the paper, Basu's experimental data (represented by ○) and Thorncroft et al.'s experimental data (denoted by ▲ and ▼) of wall temperature are used, while the wall temperatures for Situ et al.'s data (indicated with □) are estimated by using Chen's correlation [21] of two-phase heat transfer (see Appendix A):

$$q''_w = q''_{FC} + q''_{NB} = h_{FC}(T_w - T_b) + h_{NB}(T_w - T_s), \tag{26}$$

where

$$h_{FC} = 0.023 Re_f^{0.8} Pr_f^{0.4} k_f / D_H,$$
$$h_{NB} = S(0.00122)\left[\frac{(k^{0.79} C_p^{0.45} \rho^{0.49})_f}{\sigma^{0.5} \mu_f^{0.29} i_{fg}^{0.24} \rho_g^{0.24}}\right] \Delta T_s^{0.24} \Delta p^{0.75}, \tag{27}$$

where Pr_f is liquid Prandtl number, k_f is liquid thermal conductivity, $\Delta T_s = T_w - T_s$, $\Delta p = p(T_w) - p(T_s)$, and S is the suppression factor and can be approximated by

$$S = 1/(1 + 2.53 \times 10^{-6} Re_{TP}^{1.17}), \quad (28)$$

where Re_{TP} is the two-phase Reynolds number.

It is shown in the figure that for Jacob number, Thorncroft et al.'s data are all less than 10, Situ et al.'s test conditions are situated in the middle from 8 to 21, and Basu's test conditions span from 23 to 60. The higher Jacob numbers of Basu's conditions are mainly due to the higher heat flux. While for Reynolds number, on the other hand, Thorncroft et al.'s data are mostly in the range of 6000 to 1.0×10^4, Situ et al.'s data are located at liquid Reynolds number at 3.3×10^4, 4.9×10^4, and 6.1×10^4; while for Basu's experiments, the majority of the data are obtained at $Re_f = 5.1 \times 10^4$. Hence the three datasets cover an expansive scope with Ja_w from 0 to 60 and Re_f from 6000 to 1×10^5.

4.1. Comparison of existing models and correlations with existing data

Basu's experimental results and the model prediction of the bubble waiting time and growth time are plotted in Fig. 3, where the experimental data are indicated by •, and the predictions by model or correlation are represented with open symbols □, ○, Δ, and ∇. Noted that in current and the following calculations, the cavity radius, r_c, is set as 10^{-5} m [11]. The inverse of dimensionless bubble waiting time, N_{fW}, is plotted with the three non-dimensional parameters: Re_f, Ja_w, and N_{qW} in Fig. 3a–c, respectively. Since mass flux for waiting time measurement are all set as 343 kg/m^2 s, all the data and prediction in Fig. 3a reside at $Re_f = 5.1 \times 10^4$. Fig. 3b indicates that bubble waiting time decreases as the increasing of wall superheat, and all these three models/correlations have a reasonable good agreement with the experimental data. In Fig. 3c, the data are only available at $N_{qW} = 18.3$, 35.9, and 40.0, and the relationship between N_{qW} and N_{fW} is indistinguishable. Hence N_{qW} is not an appropriate parameter describing waiting time, while Jacob number is a good candidate. In addition, the empirical correlation proposed by Basu et al. only correlates waiting time with wall superheat. However, a convincible correlation comes short due to the lack of experimental data.

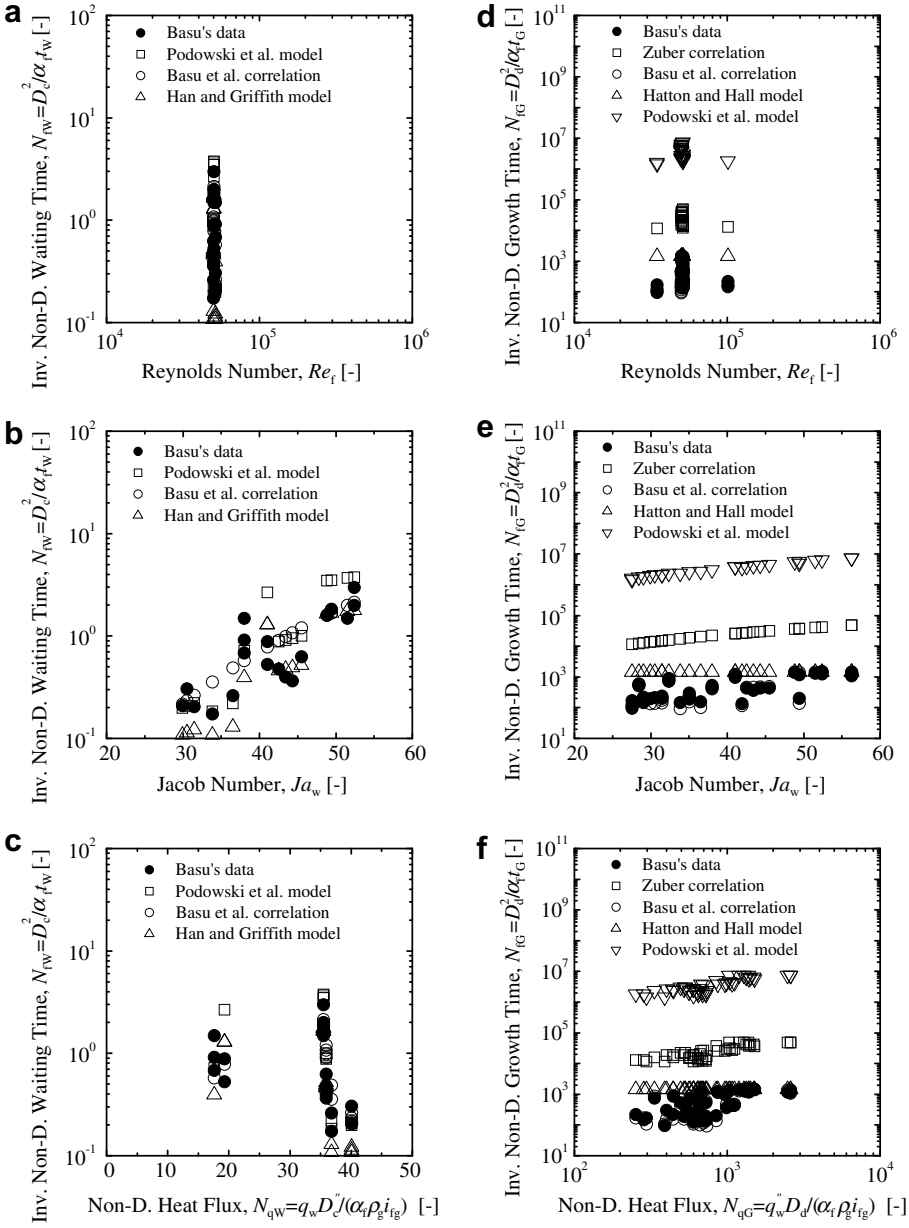

Fig. 3. Comparison of inverse of the dimensionless bubble waiting time and growth time between models and Basu's data.

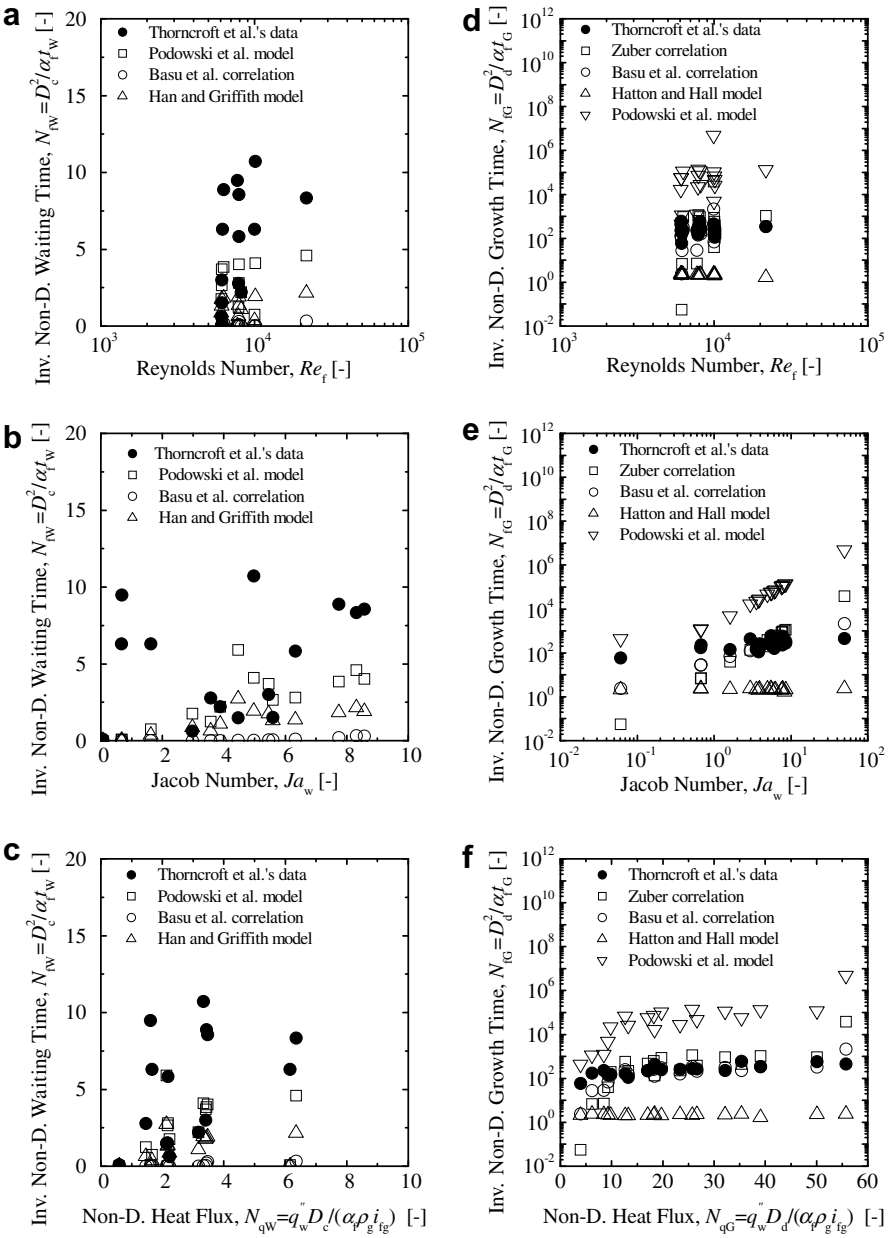

Fig. 4. Comparison of inverse of the dimensionless bubble waiting time and growth time between models and Thorncroft et al.'s data.

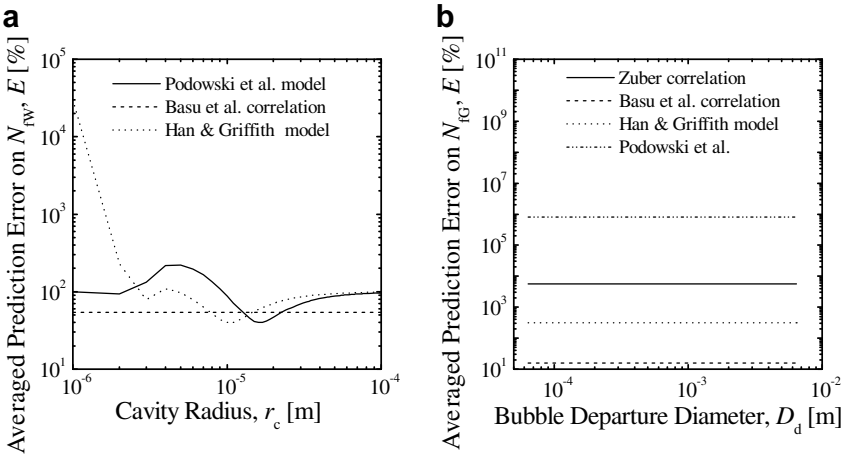

Fig. 5. Averaged prediction errors on N_{fW} and N_{fG} with varying values of r_c and D_d.

The inverse of dimensionless bubble growth time, N_{fG}, from Basu's measurement results and the prediction of the four bubble growth time models, are plotted against Re_f, Ja_w, and N_{qG} in Fig. 3d–f, respectively. Unsurprisingly, Basu et al.'s correlation agrees well with their own experimental data. Fig. 3d shows that all the data were taken at $Re_f = 3.5 \times 10^4$, 5.1×10^4, and 1.0×10^5, and the models by Zuber, Hatton and Hall, and Podowski et al. all over-predict the growth time. This can be confirmed in Fig. 3d and e. In addition, the prediction of Hatton and Hall is a constant value, because the right hand side of Eq. (7) solely depends on fluid property. The predictions by Zuber and Hatton & Hall show increasing with the growing of Jacob number, Ja_w, and dimensionless heat flux N_{qG}. This is because when the heat flux increases, the wall superheat increases, and bubble needs less growth time to reach departure diameter. However, this trend is not very clear for the experimental data due to the limited data range.

Fig. 4 shows Thorncroft et al.'s data and the corresponding prediction of bubble waiting and growth time. The formats and symbols are the same as those in Fig. 3. It is strongly suggested in the Fig. 4a–c that all of the models and correlations fail to predict the inverse of dimensionless bubble waiting time, which scatters in the three maps vs. Re_f, Ja_w, and N_{qW}. As shown in the Fig. 4d–f, the inverse of dimensionless bubble growth time shows increasing trend with the dimensionless heat flux N_{qG}, and only Basu et al.'s correlation has a reasonable agreement with the averaged uncertainty of ±58.1%.

The definitions of N_{fW} and N_{fG} suggest that they are proportional to the square power of cavity radius r_c and departure diameter D_d. To estimate the effects of r_c, N_{fW} are re-calculated with r_c changing from 10^{-6} to 10^{-4} m, and the averaged errors are plotted in Fig. 5a. The figure shows that the prediction error for Basu et al.'s correlation does not depend on cavity size, which is clear from Eq. (14). Both models of Podowski et al. and Han & Griffith has smallest error at $r_c = 10^{-5}$ m, which justifies the previous setting of r_c. Similarly, N_{fG} are calculated with r_c with D_d varies from one tenth to ten times of the measured D_d values. The averaged prediction error

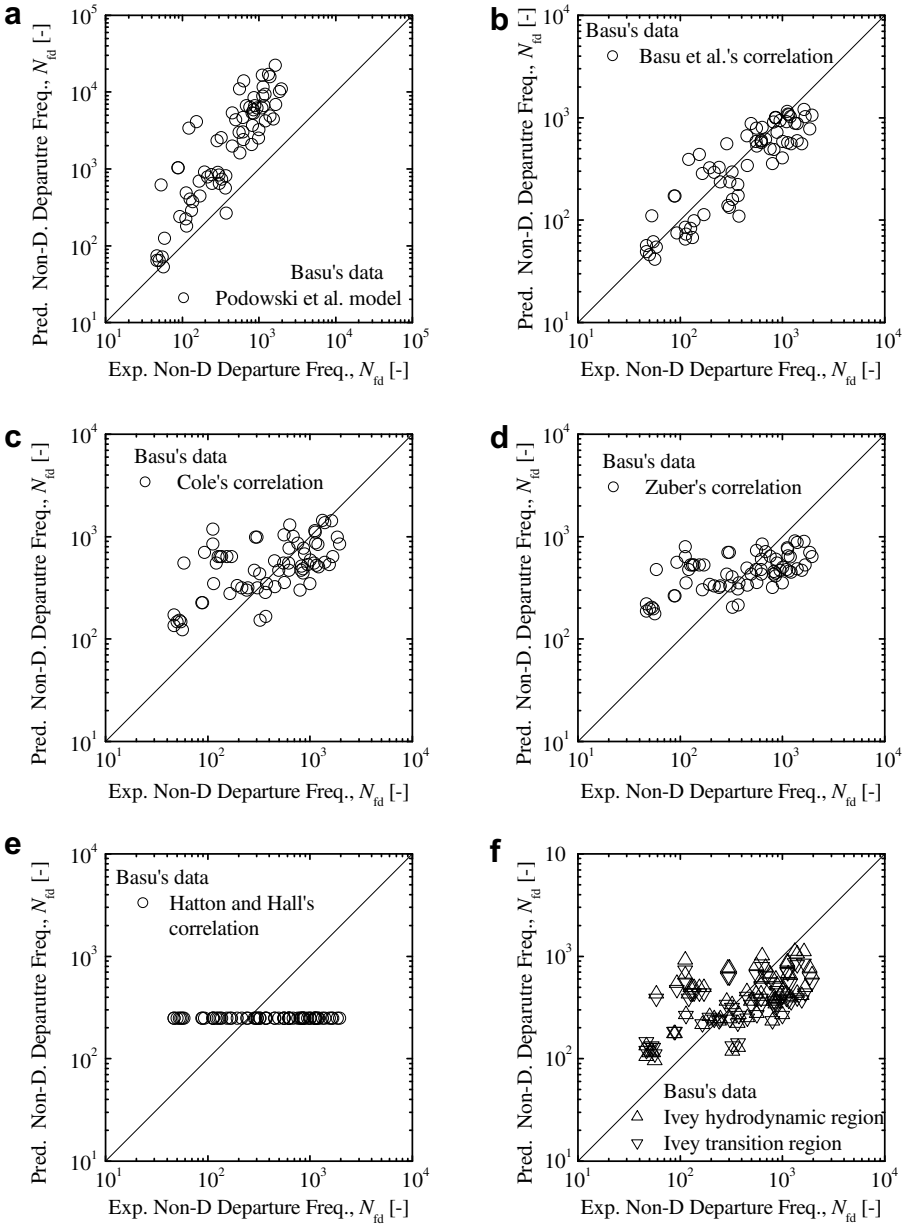

Fig. 6. Comparison of dimensionless bubble departure frequency between models and Basu's data.

shown in Fig. 5b, however, indicates that all the models do not depend on bubble departure size. This is correct since the growth time is proportional to D_d^2, thus it is cancelled out in calculating N_{fG}.

As indicated in Section 2, Podowski et al. and Basu et al. proposed model or correlation on both bubble waiting time and growth time. Their predictions of non-dimensional bubble departure frequency against the datasets of Basu, Situ et al., and Thorncroft et al. are shown in Figs. 6–8, respectively. Also listed in the figures are other correlations developed for pool boiling. The bubble departure diameters for Basu's and Thorncroft data use the measured value; whilst the bubble departure diameters for the Situ et al.'s experimental conditions are calculated by force balance, which is detailed in Appendix B. The estimation predicts the bubble departure size in the range from 0.13 to 0.59 mm, which is smaller than Basu's data in the rage of 0.16 to 1.65 mm. Fig. 6 shows that Basu et al.'s correlation agrees well with their own data. Podowski's model over-predicts the departure frequency. The predictions of Cole, Zuber, and Ivey are scattered between 10^2 and 10^3, while Hatton and Hall's correlation gives a constant value. In Fig. 7 and similarly in Fig. 8, nevertheless, Podowski et al.'s model and Basu's correlation mostly under-predict the departure frequency, while the other four correlations give scattered prediction, with majority as over-prediction. These correlations were developed for pool boiling condition. Because the liquid velocity in subcooled boiling flow is higher than 0.5 m/s, the model prediction would deviate from the data. Basu's correlation was developed for their heating surface properties and limited test conditions, and it might not work for other heating material, experimental range and working fluid. In Podowski et al.'s model, the initial liquid temperature at the moment of bubble departure is assumed to be bulk temperature, which is lower than saturation temperature. However, in actual situation, when one bubble departs, the surrounding liquid temperature might be higher than saturation temperature. The under-estimation of liquid temperature would result in longer waiting time, and lower departure frequency.

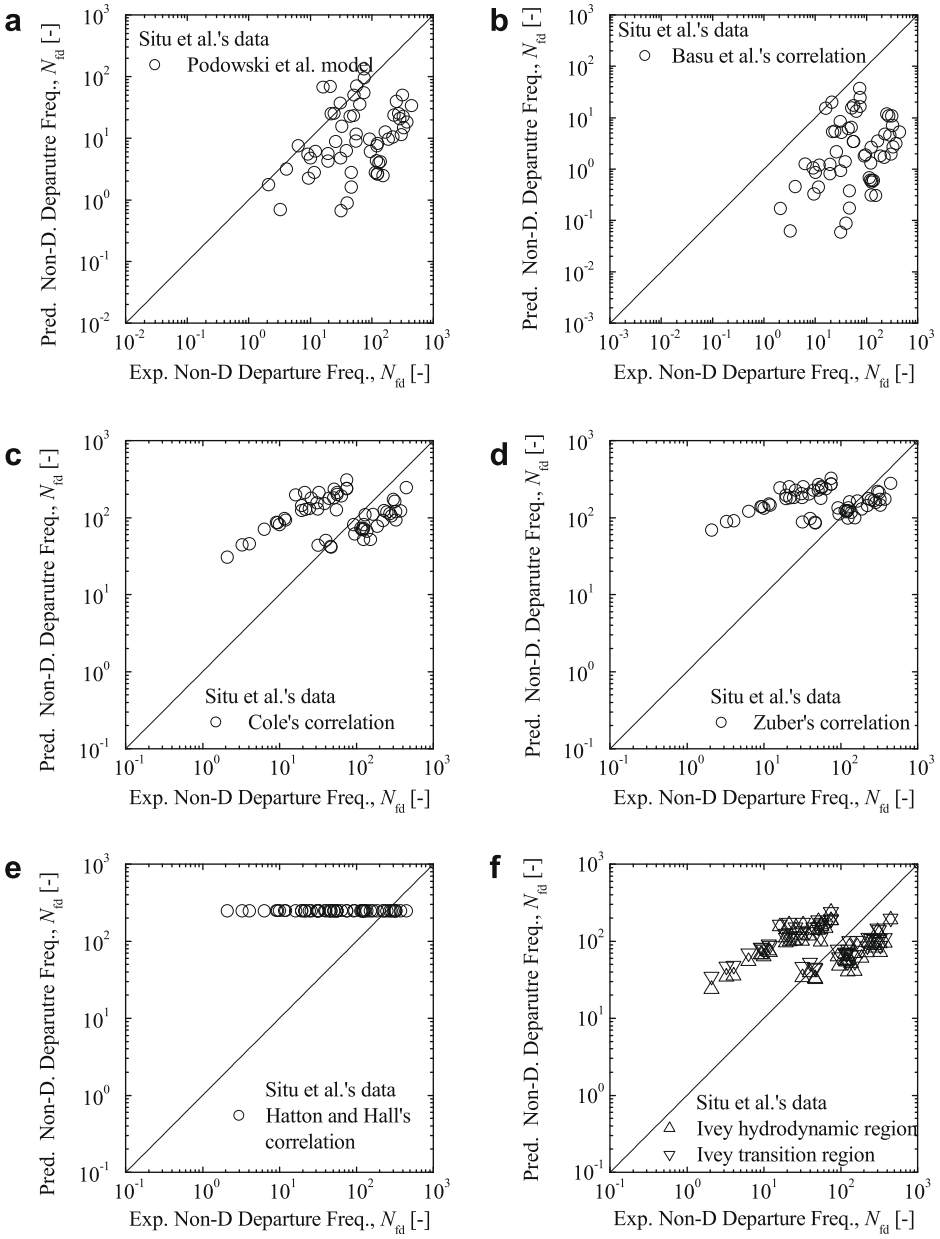

Fig. 7. Comparison of dimensionless bubble departure frequency between models and Situ et al.'s data.

In summary, the existing model or correlation cannot predict the bubble departure frequency in flow boiling. The bubble nucleation mechanism in forced convective boiling flow is far more complex than pool boiling. The assumption of hydrodynamic or thermodynamic regions, where these correlations are located, cannot describe the bubble departure in forced convective flow, which is governed by heat conduction, bubble growth, and force balance on the bubble. The two models developed for forced convective subcooled boiling flow also fail for various working fluid and experimental range. Hence it is necessary to develop a correlation suitable for the forced convective subcooled boiling, which will be discussed as follows.

4.2. Correlation derivation

Experimental observation revealed that Situ et al.'s data of bubble departure frequency were taken at partial boiling region, where nucleate boiling takes place at isolated nucleation sites. In addition, Thorncroft et al.'s measurements are located at low wall superheat. Basu's datasets were also obtained at the beginning section of subcooled boiling, because visualization would blocked if too many bubbles are presented on the heated surface [10]. In this region, most of heat is removed by forced convective heat transfer, and nucleate boiling heat transfer is relatively small [26] (the detailed discussion is presented in Appendix C). Data analysis suggests that bubble departure frequency is a weak function of Jacob number and Reynolds number and would be related to heat flux that should be appropriately chosen. Moreover, none of the combination of the dimensionless number developed based on previous correlations and models can provide a promising correlation. Appendix C indicates that bubble departure frequency is related with evaporation heat transfer, and it can be correlated with nucleate boiling heat flux. Thus, another dimensionless heat flux representing nucleate boiling heat transfer is defined as

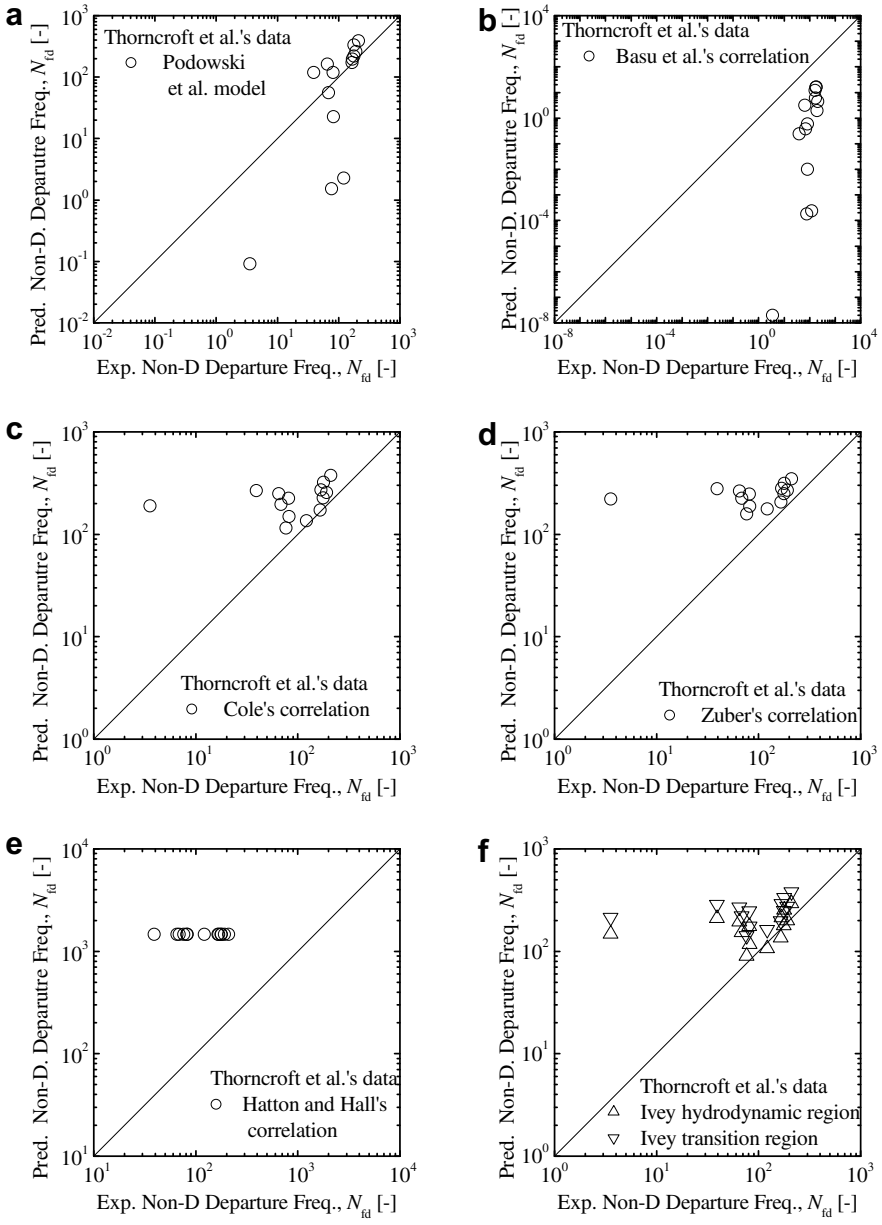

Fig. 8. Comparison of dimensionless bubble departure frequency between models and Thorncroft et al.'s data.

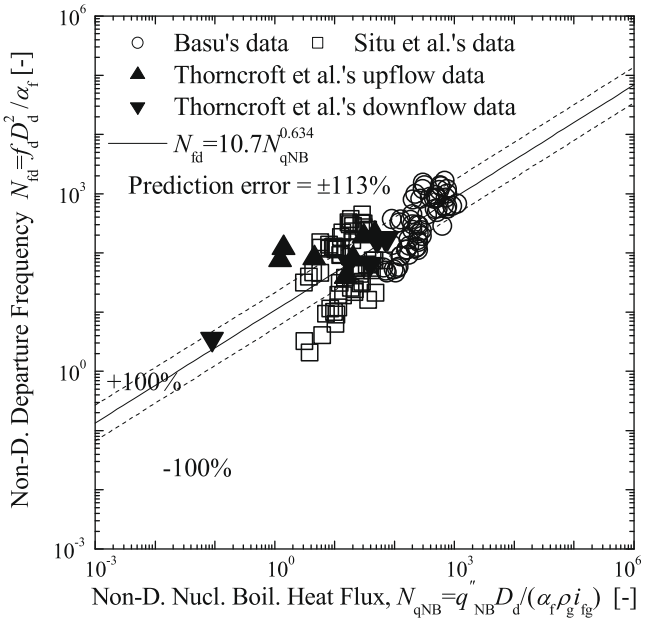

Fig. 9. Comparison between predicted and measured dimensionless bubble departure frequency.

$$N_{qNB} \equiv \frac{q''_{qNB}D_d}{\alpha_f \rho_g i_{fg}}, \tag{29}$$

where the nucleate boiling heat flux is calculated by using Chen's correlation. An empirical correlation can be derived by using least square method as

$$N_{fd} = 10.7N_{qNB}^{0.634}, \tag{30}$$

which is plotted in Fig. 9. Since the dimensionless bubble departure frequency, as well as the dimensionless nucleate boiling heat flux, covers the range from 10^{-1} to 10^3, the correlation gives an acceptable agreement, although the averaged deviation of prediction is ±113%.

To summarize, the dimensionless analysis finds that Reynolds number and Jacob number do not have a significant effect on bubble departure frequency. Wall heat flux provides for the single-phase convective heat flux and evaporation or nucleate boiling heat flux. Hence the dimensionless bubble departure frequency can be correlated with dimensionless nucleate boiling heat flux. In view of the fact that the experimental data available are mainly located at the beginning section of nucleate boiling, the application of correlation in Eq. (30) should be taken carefully. The proposed correlation is suitable for partially nucleate boiling region with Ja_w less than 60. Extension of the correlation to predict departure frequency at higher wall superheat needs the validation with more databases.

5. Conclusions

Forced convective subcooled flow boiling experiments were conducted in a vertical-upward annular channel by using water as testing fluid. The test runs were performed at atmosphere pressure. The inlet temperature ranged from 80.0 to 98.5 °C; the inlet velocity varied from 0.487 to 0.939 m/s; and the heat flux changed from 60.7 to 206 kW/m^2. A high-speed digital video camera was used to capture the bubble nucleation at partial boiling region. Bubble departure frequencies were obtained from the images for a total of 58 test conditions.

Non-dimensional analysis was performed on the present data as well as the data taken by Basu [9] and Thorncroft et al. [8]. Existing models and correlations were examined with the experimental data. The models developed from pool boiling flow do not work well for convective flow boiling. Basu et al.'s correlation only works well against her own data. The mechanistic model proposed by Podowski et al. also does not fit with the current data, due to the weakness in the model's assumption. In the partial boiling region, the bubble departure frequency is found to be related with nucleate boiling heat transfer. Hence, the non-dimension bubble departure frequency is correlated with dimensionless nucleate boiling heat flux. The proposed correlation agrees reasonably well with existing databases with low wall superheat.

Acknowledgements

The research project was supported by the Tokyo Electric Power Company (TEPCO) and Australian Research Council (ARC) Discovery Project DP0556094. The authors would like to express their sincere appreciation for the support from the TEPCO and ARC.

Appendix A. Wall surface temperature estimation

Chen's correlation is compared with other four correlations (Shah [22], Bjorge et al. [23], Gungor & Winterton [24], and Liu & Winterton [25]) in predicting Basu's Jacob number data [9] in Fig. A1. The Jacob number is proportional to wall superheat as shown in Eq. (5). A total of 130 test conditions cover the mass flux from 124 to 890 kg/m^2 s, the heat flux from 11.0 to 1130 kW/m^2, and inlet subcooling from 6.6 to 53 °C. It is indicated that the correlation of Gungor & Winterton [24] under-predicts the wall temperature, which means that the heat transfer coefficient is over-predicted. Liu & Winterton [25] gives prediction of wall temperature just above the saturation temperature due to the over-prediction of nucleate boiling heat transfer coefficient. Bjorge et al.'s correlation [23] gives good estimation of Jacob number with error of ±52.0%. Nevertheless, it does not lead to the successful modelling of bubble departure frequency. Chen's correlation [21] has been widely adopted for subcooled boiling and saturated boiling for various working fluids. Although it over-predicts the Jacob number for Basu's data (averaged error: ±68.2%), similar as Shah's correlation [22] (error: ±56.0%), it is used in this paper to estimate wall temperature for Situ et al.'s test conditions.

Appendix B. Bubble departure size estimation

Bubble departure diameter is also measured in Basu's data but not measured in the current data. In the authors' previous paper [19], the force balance of bubble at nucleation site was discussed, as shown in Fig. B1. The forces indicated in the figure, F_{sx}, F_{dux}, F_{sl}, F_{sy}, F_{duy}, F_p, F_g, and F_{qs} are the surface tension force at x-direction, the unsteady drag force (growth force) at x-direction, the shear lift force, the surface tension force at y-direction, the unsteady drag force at y-direction, the pressure force, the gravity force, and the quasi-steady force respectively. Different from the bubble lift-off, the bubble departs when it violates the force balance along the flow direction:

$$\sum F_y = F_{sy} + F_{duy} + F_p + F_g + F_{qs}. \tag{B1}$$

At the moment of bubble departure, the surface tension force can be neglected because the bubble contact area on the wall becomes zero. The growth force in the flow direction is given by [19]

$$F_{duy} = -\rho_f \pi r_b^2 \left(\frac{11}{2}\dot{r}_b^2 + \frac{11}{6} r_b \ddot{r}_b\right) \sin\theta_i, \tag{B2}$$

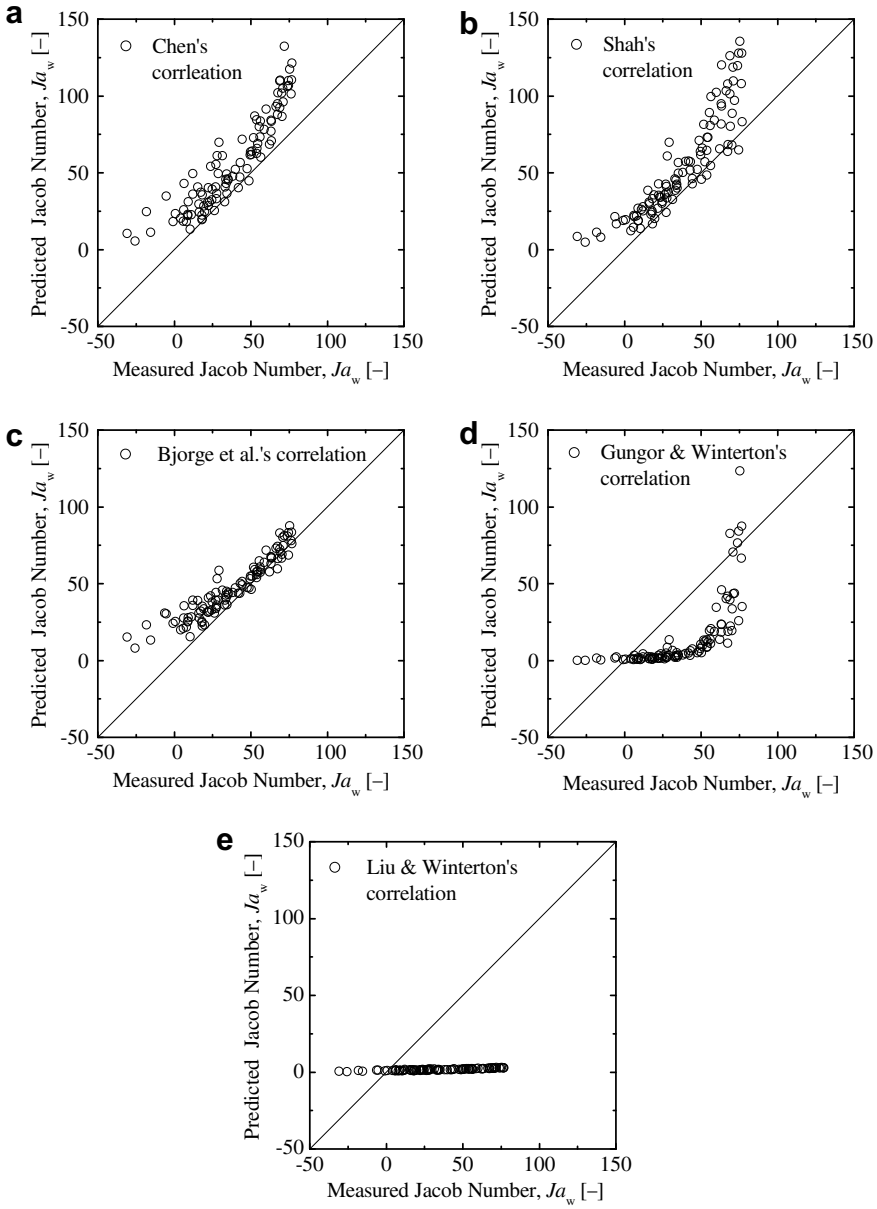

Fig. A1. Test conditions in Ja_w vs. Re_f map.

where r_b, $\dot{r}_b$, $\ddot{r}_b$, and θ_i are bubble radius, derivative of bubble radius with respect to time, and second derivative of bubble radius with respect to time, and inclination angle respectively. The inclination angle is set as $\pi/18$ [27]. By adopting the modified Zuber's bubble growth equation in Eq. (4), the growth force can be deduced as

$$F_{duy} = -\frac{44b^4\alpha_f^2}{3\pi}\rho_f Ja_e^4 \sin\theta_i. \tag{B3}$$

where the effective Jacob number is defined as

$$Ja_e \equiv \frac{\rho_f C_{pf} S(T_w - T_s)}{\rho_g i_{fg}} \tag{B4}$$

with a suppression factor counting the effect of liquid flow. Eq. (B3) suggests that the bubble growth force depends on wall superheat rather than bubble size. Furthermore, it is very sensitive to wall temperature because it is proportional to the fourth power of the effective Jacob number. The pressure, gravity, and quasi-steady forces are given as

$$F_p + F_g = \frac{4}{3}\pi(\rho_f - \rho_g)g r_b^3, \tag{B5}$$

$$\frac{F_{qs}}{6\pi\mu_f u_r r_b} = \frac{2}{3} + \left[\left(\frac{12}{Re_b}\right)^n + 0.796^n\right]^{-1/n}, \tag{B6}$$

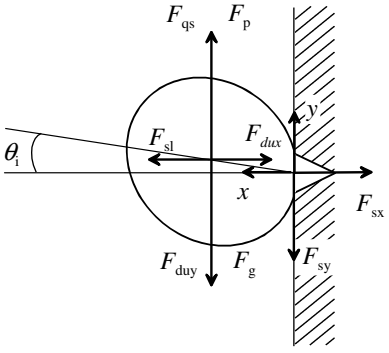

Fig. B1. Force balance of a vapor bubble at a nucleation site.

where u_r, Re_b, and n are relative velocity between phases, bubble Reynolds number, and the constant set as 0.65, respectively.

The predicted bubble departure diameter for the current test conditions are from 0.13 to 0.59 mm, which agrees with the experimental observation that the bubble departure diameters are between 0.1 and 0.4 mm. However, it is much smaller than the data taken by Basu [9], which ranges from 0.16 to 1.65 mm. To validate the calculation, the force balance analysis is also performed for Basu's test data. Although the averaged prediction error on bubble departure diameter D_d is ±228% (same prediction error for N_{qG}, which is proportional to D_d), the predicted bubble departure sizes are from 0.48 to 3.52 mm, within the same data range. Analysis also finds that bubble growth force is the most dominant force, and wall superheat has a dramatic influence on growth force. Hence, the smaller Jacob number for Situ et al.'s data, as shown in Fig. 2, produces a much smaller bubble departure size.

Appendix C. Discussion of non-dimensional parameters in partial boiling region

It has been stated in Section 4.2 that all the data were taken at partial boiling section, which is close to the point of onset of nucleation boiling (ONB). Several models in literature describe the heat flux at the ONB. Our previous study [19] found that Sato and Matsumura's correlation gives the best results:

$$q''_{ONB} = \frac{k_f \rho_g i_{fg}}{8\sigma T_s}(T_w - T_s)^2. \tag{C1}$$

The dimensionless numbers representing wall superheat and heat flux are Ja_w, and N_{qW} or N_{qG}. In Figs. 3 and 4, N_{qW} does not have clear influence on bubble waiting time. Hence, the other dimensionless heat flux number, N_{qG}, is drawn with Jacob number for Basu', Situ et al.', and Thorncroft et al.'s data (represented by ○, □, ▲ and ▼respectively) in Fig. B1. It is interesting to find that the experimental data are in the parabolic shape. By using with least square method, the data can be approximated by

$$N_{qG} = 5.28 Ja_W^{1.37}, \tag{C2}$$

which is plotted as the solid curve in Fig. C1. The figure indicates that this curve agrees well with all datasets with prediction uncertainty of ±46.7%. Note that in the above equation, the power on the wall superheat is 1.37, which is close to the power of 2, as shown in Eq. (C1).

Next is to find the relationship between dimensionless heat flux and dimensionless bubble departure frequency. In literature, many researchers separated the heat flux into two parts: forced convective and nucleate boiling heat flux. Recently, Basu et al. [10] divided the heat flux into two components: heat flux to liquid q''_l, and heat flux for evaporation q''_{ev}. The evaporation heat flux is give by

$$q''_{ev} = \frac{N_a}{A_h} f_d \frac{\pi}{6} D_d^3 \rho_g i_{fg}, \tag{C3}$$

where N_a and A_h are active nucleation site density and heated area. The heat transfer to liquid consists of the force convective heat transfer and the condensation from bubble top. If the condensation heater transfer from the bubble top is neglected, the heat flux through an area of size $\frac{\pi}{4}D_d^2$ under a nucleation cavity can be given as

$$q''_w \frac{\pi}{4} D_d^2 = (1 - C_{ev}) q''_{FC} \frac{\pi}{4} D_d^2 + C_{ev} f_d \frac{\pi}{6} D_d^3 \rho_g i_{fg}, \tag{C4}$$

where a coefficient C_{ev} is introduced to count for the percentage of micro-layer area over the area of size $\frac{\pi}{4}D_d^2$. Heat transferred within the micro-layer area provides the energy for evaporation, while heat transfer through the rest of the area goes for the convective heat transfer to liquid. The non-dimensionalization of the above equation leads to

$$\frac{q''_w D_d}{\alpha_f \rho_g i_{fg}} = (1 - C_{ev}) \frac{q''_{FC} D_d}{\alpha_f \rho_g i_{fg}} + \frac{2}{3} C_{ev} \frac{f_d D_d^2}{\alpha_f} \tag{C5}$$

or

$$N_{qG} = (1 - C_{ev}) N_{qFC} + 2 C_{ev} N_{fd}/3. \tag{C6}$$

where the dimensionless single-phase forced convective heat flux is defined as

$$N_{qFC} \equiv \frac{q''_{FC} D_d}{\alpha_f \rho_g i_{fg}} \tag{C7}$$

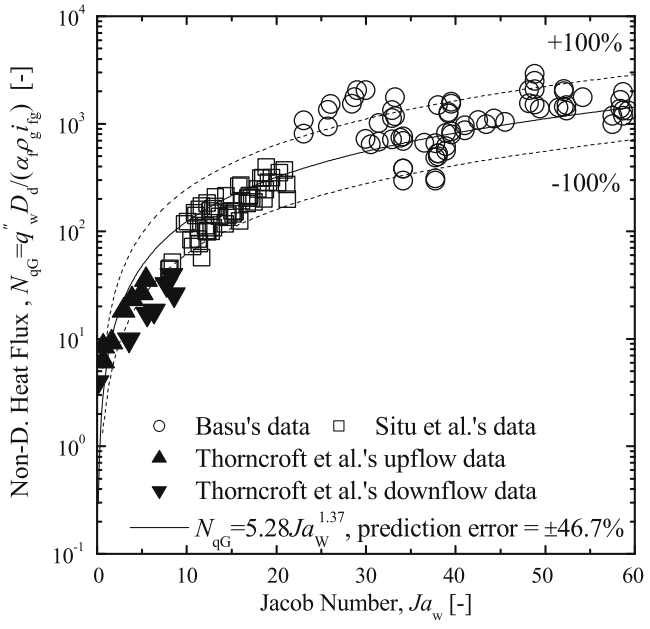

Fig. C1. Dependence of dimensionless heat flux on Jacob number.

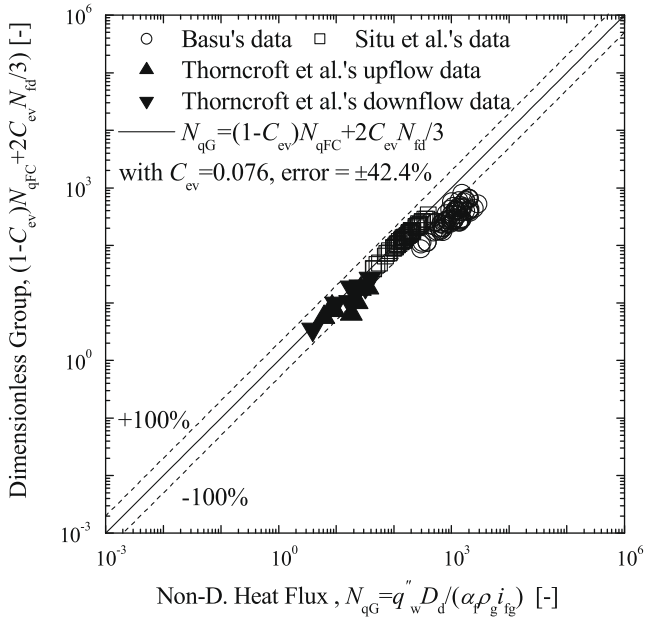

Fig. C2. Dependence of dimensionless group $[(1 - C_{ev})N_{qFC} + 2C_{ev}N_{fd}/3]$ with $C_{ev} = 0.076$ on dimensionless heat flux.

and the forced convective single-phase heat flux is calculated by Eq. (27). By fitting with experimental data, the minimum averaged error ±42.4% appears when coefficient C_{ev} is equal to 0.076, which means that the micro-layer area accounts for less than 10% of the bubble area. Fig. C2 plots the dimensionless group $[(1 - C_{ev})N_{qFC} + 2C_{ev}N_{fd}/3]$ with $C_{ev} = 0.076$ against dimensionless heat flux N_{qG}. The figure shows that Eq. (C6) has a fairly well agreement with all the three datasets.

References

[1] N. Zuber, Hydrodynamic aspects of boiling heat transfer, US AEC Rep. AECU 4439, Tech. Inf. Serv. Oak Ridge, Tenn. 1959.
[2] N. Zuber, Recent trends in boiling heat transfer research Part I: nucleate pool boiling, Appl. Mech. Rev. 17 (1964) 663–672.
[3] M. Jakob, Heat Transfer, vol. 1, Wiley, New York, 1949 (Chapter 29).
[4] N. Zuber, Nucleate boiling. The region of isolated bubbles and the similarity with natural convection, Int. J. Heat Mass Transfer 6 (1963) 53–78.
[5] H.J. Ivey, Relationships between bubble frequency, departure diameter and rise velocity in nucleate boiling, Int. J. Heat Mass Transfer 10 (1967) 1023–1040.
[6] C.Y. Han, P. Griffith, The mechanism of heat transfer in nuclear pool boiling – Part I. Bubble initiation, growth and departure, Int. J. Heat Mass Transfer 8 (1965) 887–904.
[7] A.P. Hatton, I.S. Hall, Photographic study of boiling on prepared surfaces, in: Third International Heat Transfer Conference, vol. 4, Chicago, Illinois, USA, August 7–12, 1966, pp. 24–37.
[8] G.E. Thorncroft, J.F. Klausner, R. Mei, An experimental investigation of bubble growth and detachment in vertical upflow and downflow boiling, Int. J. Heat Mass Transfer 41 (1998) 3857–3871.
[9] N. Basu, Modeling and experiments for wall heat flux partitioning during subcooled flow boiling of water at low pressures, Ph.D. Thesis, University of California, Los Angeles, USA, 2003.
[10] N. Basu, G.R. Warrier, V.K. Dhir, Wall heat flux partitioning during subcooled flow boiling: Part1– model development, J. Heat Transfer 127 (2005) 131–139.
[11] R.M. Podowski, D.A. Drew, R.T. Lahey Jr., M.Z. Podowski, A mechanistic model of the ebullition cycle in forced convection subcooled boiling, in: Eight International Topical Meeting on Nuclear Reactor Thermal-Hydraulics, vol. 3, 1997, pp. 1535–1542.
[12] N. Zuber, The dynamics of vapor bubbles in nonuniform temperature fields, Int. J. Heat Mass Transfer 2 (1961) 83–98.
[13] L.Z. Zeng, J.F. Klausner, D.M. Bernhard, R. Mei, A unified model for the prediction of bubble detachment diameters in boiling systems - II. Flow boiling, Int. J. Heat Mass Transfer 36 (1993) 2271–2279.
[14] M.S. Plesset, S.A. Zwick, The growth of vapor bubbles in superheated liquids, J. Appl. Phys. 25 (1954) 493–500.
[15] R. Cole, A photographic study of pool boiling in the region of the critical heat flux, AIChE J. 6 (1960) 533–542.
[16] R. Situ, T. Hibiki, X. Sun, Y. Mi, M. Ishii, Flow structure of subcooled boiling flow in an internally heated annulus, Int. J. Heat Mass Transfer 47 (2004) 5351–5364.
[17] R. Situ, T. Hibiki, X. Sun, Y. Mi, M. Ishii, Axial development of subcooled boiling flow in an internally heated annulus, Exp. Fluids 37 (2004) 589–603.
[18] R. Situ, Y. Mi, M. Ishii, M. Mori, Photographic study of bubble behaviors in forced convection subcooled boiling, Int. J. Heat Mass Transfer 47 (2004) 3659–3667.
[19] R. Situ, T. Hibiki, M. Ishii, M. Mori, Bubble lift-off diameter in forced convective subcooled boiling, Int. J. Heat Mass Transfer 48 (2005) 5536–5548.
[20] R. Situ, Experimental and theoretical investigation of adiabatic bubbly flow and subcooled boiling flow in an annulus, Ph.D. Thesis, Purdue University, West Lafayette, IN, USA, 2004.
[21] J.C. Chen, Correlation for boiling heat transfer to saturated fluids in convective flow, I& EC Proc. Des. Dev. 5 (1966) 322–329.
[22] M.P.E. Shah, A general correlation for heat transfer during subcooled boiling in pipes and annuli, ASHRAE Trans. 83 (1977) 202–217.
[23] R.W. Bjorge, G.R. Hall, W.M. Rohsenow, Correlation of forced convection boiling heat transfer data, Int. J. Heat Mass Transfer 25 (1982) 753–757.
[24] K.E. Gungor, R.H.S. Winterton, A general correlation for flow boiling in tubes and annuli, Int. J. Heat Mass Transfer 29 (1986) 351–358.
[25] Z. Liu, R.H.S. Winterton, A general correlation for saturated and subcooled flow boiling in tubes and annuli, based on a nucleate pool boiling equation, Int. J. Heat Mass Transfer 34 (1991) 2759–2766.
[26] N.E. Fagerholm, A.R. Ghzzanfari, K. Kivioja, Boiling heat transfer in a vertical tube with Freon 114, Heat Mass Transfer 17 (1983) 221–232.
[27] J.F. Klausner, R. Mei, D.M. Bernhard, L.Z. Zeng, Vapor bubble departure in forced convection boiling, Int. J. Heat Mass Transfer 36 (1993) 651–662.